Temperature-Dependent Femtosecond Photoinduced Desorption in CO/Pd(111)[†]

Paul Szymanski, Alex L. Harris, and Nicholas Camillone III*

Chemistry Department, Brookhaven National Laboratory, Upton, New York 11973-5000

Received: July 26, 2007; In Final Form: August 27, 2007

The desorption of CO from a Pd(111) surface following absorption of 120 fs pulses of 780 nm light occurs on two distinct and well-separated time scales. Two-pulse correlation measurements show a fast subpicosecond decay followed by a slower, ∼40 ps decay. Simulations based on the two-temperature model of electron and phonon heat baths within the substrate, and an empirical friction model to treat coupling to the adsorbate, support the assignment of the desorption mechanism as an electron-mediated process. The photodesorption yield and overall width of the temporal response exhibit a marked dependence on the initial surface temperature in the 100–375 K range despite the much higher transient electronic temperatures (∼7000 K) achieved. The observed temperature dependences can be attributed directly to variations in the initial temperature within the frictional coupling picture. Simulations of this extended data set imply that the activation barrier to photoinduced desorption is equal in magnitude to that derived from thermal desorption experiments for this system within the limits of a one-dimensional Arrhenius desorption model. The simulations also imply that the slower decay is not the result of phonon-driven desorption. Though we cannot unambiguously determine the strength of the adsorbate–phonon coupling, our results suggest that its role is to moderate the degree of the adsorbate excitation.

1. Introduction

In recent years, the direct time-domain investigation of various physicochemical transformations at surfaces has been addressed by a number of different ultrafast laser-based techniques.[1] A primary focus has been on photoinduced desorption. Cleavage of the molecule–surface bond is arguably the simplest surface chemical reaction, analogous to unimolecular bond dissociation in the gas phase. On this basis photoinduced desorption serves as a starting place for time-resolved studies directed at understanding the dynamics fundamental to a microscopic understanding of surface chemical transformations such as those involved in heterogeneous catalysis and photocatalysis. However, identifying the mechanisms and quantifying the interactions underlying the dynamics remains an experimental and theoretical challenge.

One of the most important and well-studied surface chemical processes in this area of inquiry is electron-mediated photoinduced desorption. We limit our discussion here to the case where adsorbed molecules do not absorb the incident light, so the absorbed energy is initially confined to the substrate electrons. Thus, desorption is driven by interaction between the adsorbate and the excited substrate electron distribution. This class of photoinduced surface chemistry is a type of DIET (desorption induced by electronic transition)[2–6] and in its simplest form is understood as the result of transfer of an excited electron (or hole) from the substrate into a molecular orbital. Relaxation of the adsorbate–substrate complex along a repulsive excited-state potential[7,8] or a repulsive region of the ground-state potential[9] converts the energy of the electronic excitation into kinetic energy, cleaving the molecule–surface bond with a probability that is a factor of ∼10^3 smaller than dissociative electron attachment in the gas phase.[10,11] The relative inefficiency of

DIET on metal surfaces is attributed to short molecular resonance lifetimes due to the degeneracy of the molecular affinity level with the substrate conduction band.

When the substrate electronic excitation is driven by picosecond or shorter pulses of sufficient energy density,[12,13] a large degree of electronic excitation can be achieved without exceeding the damage threshold of the metal. The excited carrier density is then sufficiently large that multiple cycles of adsorbate electronic excitation and de-excitation can occur before the substrate electronic system relaxes. Because the resonance lifetime is short, each cycle is believed to involve transfer of a single electron. Each cycle leaves the molecule–surface bond in a vibrationally excited state. Repeated excitations into the resonance before vibrational relaxation occurs can deposit sufficient energy into the bond for the molecule to desorb.[6] This process is known as DIMET (desorption induced by multiple electronic transitions), and it gives rise to significantly enhanced desorption probabilities compared to DIET.[12–14]

Alternatively, interactions between the adsorbate nuclear degrees of freedom and electron–hole pairs (EHPs) within the substrate may drive desorption. Such a mechanism is envisioned as the reverse of EHP-mediated adsorbate vibrational relaxation, wherein energy flows from the adsorbate to the substrate.[4,5,15–18] In the case of desorption, it is believed that energy released by EHP annihilation events is transferred from the substrate to the adsorbate, progressively exciting the molecule–surface vibration and resulting in bond cleavage.[4,19] Unlike DIET and DIMET, this mechanism is understood to be adiabatic with respect to molecular electronic states, and the phenomenon is known as electronic friction to distinguish it from the analogous interactions between molecular degrees of freedom and lattice phonons.

Based on such mechanisms, numerous models have been employed to describe ultrafast photoinduced desorption, with varying degrees of complexity and success.[5] From a chemical point of view, it is most desirable to find links relating laser-

---

Temperature-Dependent Photoinduced Desorption

J. Phys. Chem. A, Vol. 111, No. 49, 2007 **12525**

driven time-resolved experiments to thermal processes such that the dynamical insights garnered from the former may be connected to the real-world processes involving the latter. A direct link between the two is, in fact, implicit in models that treat photoinduced phenomena as activated processes in a one-dimensional (single reaction coordinate) model.[5,19,20] In some such models, the overall process can be thought of in terms of two steps—vibrational excitation and desorption. The vibrational excitation process may be modeled quantum mechanically[21] or with electronic and/or lattice frictions within a master equation framework.[22] The desorption step is modeled as the crossing of an effective activation energy barrier either governed by bound-to-continuum transitions in the quantum-mechanical approach or an Arrhenius expression in the friction approach. In either approach, a simple one-dimensional potential energy surface is assumed; the activation energy is presumed to be the same as that used to describe thermal desorption.[23,24] Few studies, however, have systematically varied properties of a well-defined system to test the robustness of this assumption and the desorption parameters employed. One way in which the connection between photoinduced and thermal desorption can be tested more concretely is to vary the energy of the system on a time scale far removed from the nonequilibrium excitation. In other words, both the equilibrium and nonequilibrium excitations are controlled independently by using a combination of thermal and laser-induced heating. We will show that this approach allows the effective ground-state potential describing the molecule—surface complex and the degree of molecule—surface coupling to be established with a greater degree of certainty than can be achieved by controlling the photoinduced excitation alone.

Thus, experiments described in this work measure the dependence of the photodesorption dynamics on the base thermal temperature. Our analysis aims to identify the nature of the desorption mechanism (i.e., determine the roles played by electronic and lattice coupling) and use the results to extract the energetics and kinetics of the photodesorption event in the subpicosecond photoexcitation regime. Carbon monoxide on Pd(111) is an excellent model system for such an investigation. Adsorption at 380 K results in the formation of a well-defined $(\sqrt{3} \times \sqrt{3})$R30° 0.33 ML overlayer with CO adsorbed in 3-fold hollow sites.[25−28] The 380 K onset of thermal desorption of this structure provides a broad range of readily accessible substrate temperatures that is necessary for our study of the dependence of the photodesorption dynamics on the base surface temperature. In addition, CO is perhaps the prototypical molecular adsorbate for studies of chemistry on metal surfaces, and extensive experimental and theoretical investigations have examined its adsorption, binding energy, surface structure, and thermal oxidation on Pd.[29,30] Studies have also shown photo-enhanced CO oxidation rates on Pd.[11,31]

Our results show that the photoyield—and its dependences on the absorbed laser fluence and the delay time between pulses in a two-pulse correlation scheme—are significantly affected by changes in the initial substrate temperature. We adopt a simple empirical model of the photoinduced desorption and show that it satisfies globally the entire series of experiments by incorporating an electronic friction that depends on the substrate electronic temperature. Furthermore, systematic variation of the desorption and empirical friction parameters is used to place bounds on the physical quantities and assess the limitations of the model. The simulations of the extended data set imply that the activation barrier to photoinduced desorption is, within experimental uncertainty and the limitations of the model, equal
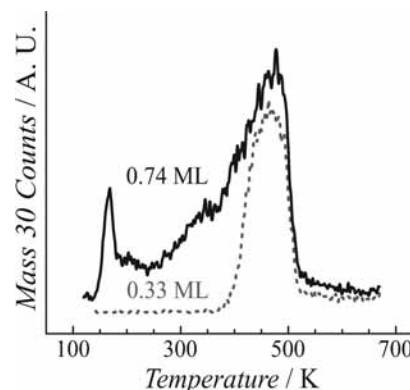

Figure 1. Temperature-programmed desorption of $C^{18}O$/Pd(111) with a heating rate of 2.5 K s^{-1}. Both the saturated surface (0.74 ML) and $(\sqrt{3} \times \sqrt{3})$R30° (0.33 ML) coverages are shown.

in magnitude to that derived from thermal desorption experiments for this system. We also discuss the physical origins and implications of our proposed electron-mediated desorption mechanism and compare the dynamics with CO photodesorption measurements on other metal substrates.[23,24,32,33]

2. Experimental Methods

A complete description of the experimental apparatus and procedure is available elsewhere.[34] The Pd(111) single-crystal substrate is maintained in ultrahigh vacuum and prepared prior to each experiment by Ar$^+$ sputtering, annealing, and oxygen treatment. Finally, the surface is exposed to a saturation dose of oxygen at room temperature and heated to perform temperature-programmed desorption (TPD). The dose-TPD cycles are repeated until desorbing CO and CO$_2$ are below detectable levels. Isotopically labeled carbon monoxide ($^{12}C^{18}O$, 95% ^{18}O substitution, 99% pure, Isotec), purified in a liquid-nitrogen-cooled trap, was introduced into the chamber via a stainless steel dosing tube that can be translated up to the face of the crystal. A $(\sqrt{3} \times \sqrt{3})$R30° structure was observed by low-energy electron diffraction (LEED) of the CO-saturated surface at 380 K. The resulting TPD spectrum (Figure 1) was assigned to a coverage of 0.33 monolayers (ML).[25,26,28] Based on this calibration, the saturation coverage at 135 K is 0.74 ML, consistent with the literature.[35]

The photodesorption experiments are performed with a regeneratively amplified Ti:sapphire laser system (780 nm, ~120 fs sech^2 pulses, 0.7 mJ/pulse) operated at a repetition rate of 8 Hz. The output of this system is divided into two orthogonally polarized beams with a variable delay between them (Figure 2). Light encountering the fixed retroreflector is p-polarized; s-polarized light traverses the variable-length path. The laser polarization is rotated prior to the beam splitter (by a half waveplate, not shown) to adjust the relative intensity of the p- vs s-polarized components and thus the relative energy from each beam absorbed by the target substrate. The p-to-s absorbed-energy ratio in our experiments was chosen to be ~1.45:1. A variable attenuator controls the total intensity of both beams, and a computer-controlled shutter regulates the admittance of the laser beams into the chamber. In all experiments, the s- and p-polarized beams are spatially overlapped and focused to a diameter of ~0.6 mm at the surface. Reflected light exits the chamber and is measured by an energy meter on a shot-to-shot basis. A quadrupole mass spectrometer (QMS) detects the photodesorbed species. To measure the dependence of the photodesorption signal on absorbed laser fluence (energy per unit area), the two beams are used with zero time delay
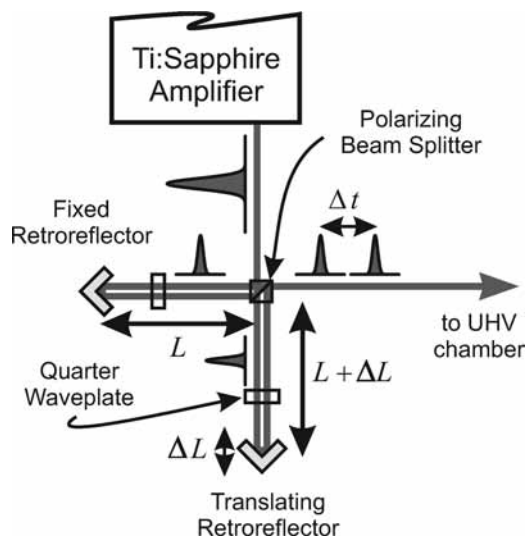
Figure 2. Schematic view of the optical delay setup for the two-pulse correlation experiments.

between them while the total incident energy is adjusted. In the two-pulse correlation (2PC) experiments, the photodesorption yield is measured as a function of the delay between the pulses of the s- and p- polarized beams. We adopt the convention that positive delays refer to the case where the more weakly absorbed s-polarized pulse arrives at the surface first. In all cases, a laser "shot" is the arrival of a single pair of pulses consisting of one from each beam. The first-shot yield, Y_{FS}, comes from the first pulse pair to arrive at the surface after the shutter is opened and gives the maximum photodesorption signal. In general, the yield decreases exponentially with an increasing number of laser shots.

For all photodesorption measurements, the surface was saturated and briefly annealed at 380 K, after which the temperature was lowered and maintained at a constant value prior to opening the shutter. No change in the bulk crystal temperature is observed during laser irradiation at 8 Hz. After ∼120 laser shots, the shutter is closed and the crystal is translated to a new position to perform the next photodesorption measurement on an undepleted region of the surface. When no suitable spots remain on the surface, TPD is performed to clean the surface before redosing. At an initial surface temperature of 135 K, the desorption yield asymptotically approaches zero after ∼100 shots, indicating that the illuminated area is completely depleted of CO. In addition, we find that the total desorption yield from ∼120 consecutive shots scales linearly with initial coverage. Thus the total desorption yield can be used to express the QMS signals in terms of monolayers. At temperatures above 135 K, the asymptotic yield following many shots is nonzero and increases with surface temperature, suggesting diffusion of chemisorbed CO into the illuminated area. Therefore, the conversion of QMS ion counts to monolayers was based solely on data acquired at 135 K, where diffusion into the illuminated area did not contribute significantly to the total desorption yield.

3. Results

Figure 3 shows the dependence of the first-shot photodesorption yield, Y_{FS}, on the initial surface temperature, T_i, over the range 85−375 K, with an initial coverage of 0.33 ML at a total absorbed fluence of 23.5 mJ cm^{-2}. The effects of surface diffusion at higher temperatures, as described in the previous section, preclude direct measurement of the cross section in the
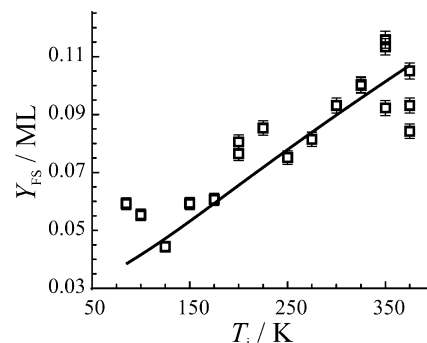

Figure 3. Photodesorption of 0.33 ML C^{18}O/Pd(111) performed at zero delay time as a function of initial temperature T_i. The line shows the result of simulations as described in the text.
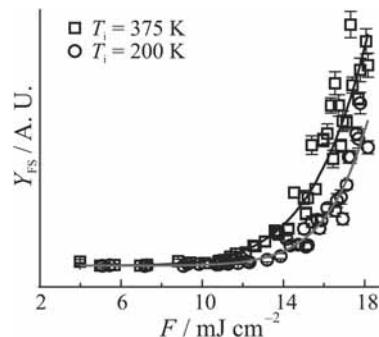

Figure 4. Fluence-dependent photodesorption of 0.33 ML C^{18}O/Pd-(111) performed at zero delay time and two initial temperatures (T_i). Lowering T_i reduces the desorption yield (symbols) while raising the power-law exponent n that empirically describes the process (solid curves). In this data, n is 6.7 (8.8) for T_i = 375 K (200 K).

usual way.[20,33,34,36] Nevertheless, we are able to express the first shot yield in monolayer units and the desorption probability in absolute terms (Y_{FS} divided by the initial coverage) by calibration at low surface temperatures where diffusion is negligible (see previous section). The yield shows a marked approximately linear factor of 3 increase over the entire range of temperatures.

The increase in yield with initial temperature (Figure 3) is accompanied by changes in the fluence dependence of the yield (Figure 4) as well as the characteristic relaxation times of the surface excitation as probed by 2PC measurements (Figure 5). Specifically, with increasing initial temperature we observe a decrease in the degree of nonlinearity of the fluence dependence and a decrease in the overall relaxation rate of the surface excitation. In the following paragraphs we discuss each of these effects in turn.

Generally, under femtosecond-pulse excitation, the first-shot yield depends on the absorbed fluence in a highly nonlinear fashion (Figure 4). Empirically, the fluence dependence may be described by a power law, $Y_{FS} \propto F^n$. Typically, $n > 3$ for photodesorption with subpicosecond pulses,[33,36,37] consistent with a mechanism where high transient adsorbate temperatures, which may greatly exceed the thermal-desorption temperature, are needed to drive the photodesorption process. For CO/Pd-(111), we find that n decreases as T_i is raised. From the data in Figure 4, n is 8.8 and 6.7 at initial temperatures of 200 and 375 K, respectively, with an experimental uncertainty of approximately 1.1. These results are consistent with the observed increase in yield with temperature at constant fluence (Figure 3); at higher initial temperatures the photodesorption is more efficient; thus the degree of nonlinearity of the fluence dependence decreases. It is likely that the decrease in n and increase in photodesorption efficiency observed here with increasing temperature reflects a strong dependence of the

Temperature-Dependent Photoinduced Desorption

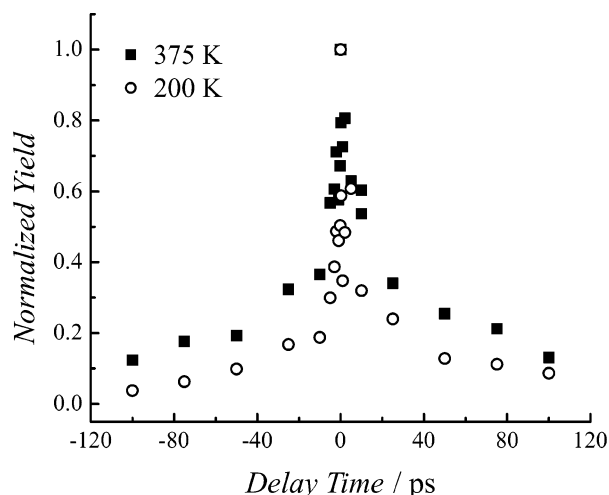*J. Phys. Chem. A, Vol. 111, No. 49, 2007* **12527**

Figure 5. First-shot yields from 2PC measurements performed at two different initial temperatures. Each data set is normalized to unity at zero delay. A slower decay of the correlation signal is observed at the higher initial temperature (375 K, closed symbols) compared to the identical measurement made at a lower temperature (200 K, open symbols). The weak signal at the longest delays is largely due to the actions of two separate, uncorrelated pulses. The slight asymmetry with respect to zero delay time is due to the use of pulses of unequal absorbed fluence (see text).

photodesorption efficiency on the initial level of thermal excitation of the adsorbate−substrate complex (see Discussion below). We believe that this effect is analogous to that observed in studies of the coverage dependence of the photodesorption yield of O_2 from Pd, where an increasing coverage correlated with a decreasing activation energy for desorption, E_a.[34] In that study, the increase in the photodesorption efficiency with decreasing E_a was linked to a decrease in the degree of nonlinearity with increasing coverage. We will consider the link between initial surface temperature and desorption efficiency quantitatively in the Discussion.

The dynamics of energy flow in the adsorbate−substrate complex can be probed in real time by two-pulse correlation measurements of the desorption yield. In such measurements, the 780 nm excitation pulse is split into two parts separated by a delay, and the photodesorption yield is measured as a function of the delay as described in the Experimental Methods. Because the absorption of the light by CO is negligible at this wavelength, the energy absorbed in the substrate must be transferred to the desorption reaction coordinate through coupling of the substrate electrons and/or phonons to the adsorbate−substrate vibrational modes.[4,23,33] The strengths of the couplings among the various degrees of freedom of the system determine the time response of the system to femtosecond-pulse excitation. By varying the delay between the two excitation pulses, the relaxation time scale(s) of the excitation driving the desorption can be measured. When a sufficiently short relaxation time, less than ∼1 ps, is observed, strong coupling of the adsorbate to the electronic degrees of freedom of the substrate is indicated. More quantitative information can be inferred by numerical simulation of the 2PC measurements based on a physical model for the desorption dynamics, as described in the Discussion.

The 2PC measurements for 0.33 ML coverage at both 375 and 200 K are shown in Figure 5. The normalized data clearly show that the overall decay is markedly slower at higher T_i. At both temperatures, the decay is well-approximated by a biexponential[34] on either side of time zero. The fast response is fit with a 0.6 ps time constant and indicates a strong coupling to the substrate electronic excitation. The slow response is fit with

30 and 50 ps time constants at 200 and 375 K, respectively. The differences in the full width at half-maximum (fwhm) of the 2PC measurements are significant: ∼3 ps at 200 K vs ∼20 ps at 375 K. The biexponential fits show that this broadening is largely due to an increased amplitude of the slow component at 375 K.

Although interpretation of the initial subpicosecond decay as indicative of an efficient electron-mediated process is straightforward,[34,38,39] the cause for the slower decay is not readily apparent. Coupling solely to lattice phonons would result in a slow decay, as the time scales for phonon excitation and relaxation are at least 1 order of magnitude slower than electron relaxation times.[33,40] Thus the ∼40 ps decay time could indicate a secondary desorption process driven by a phonon-mediated mechanism. Alternatively, a weak coupling to electrons could give rise to dynamics on this time scale, in contrast to the relatively strong coupling required for subpicosecond decays. In either case, the increased yield with increasing T_i suggests a thermally assisted barrier crossing that is effective in both the subpicosecond and ∼40 ps regimes, and the T_i dependence of the 2PC indicates that the relative significance of the contribution from the slower channel increases with initial temperature. In the next section, we discuss the results of numerical simulations that strongly support an electron-mediated desorption mechanism on both time scales, while considering the possibility that phonons may play a secondary role.

4. Discussion

In the following discussion we consider a physical model, based on frictional coupling, that is able to explain the temperature-dependent trends in the photoyield, the degree of nonlinearity of the fluence dependence, and the time-resolved dynamics experiments. The model enables us to infer the relative importance of the roles of coupling of the adsorbate to the electronic and lattice degrees of freedom of the substrate, suggesting that the desorption is exclusively driven by coupling to the substrate electronic excitation, and that the role of coupling to phonons, if any, is to moderate the degree of adsorbate excitation. The physical picture that emerges from the model is that all of the observed temperature-dependent effects can be explained by the thermal increase in the degree of vibrational excitation in the desorption coordinate with increasing initial temperature which brings the adsorbate closer to the top of the energetic barrier for photodesorption. Furthermore, we find that the activation barrier to photoinduced desorption is, within experimental uncertainty and the limitations of the model, equal in magnitude to that derived from thermal desorption experiments for this system. Finally, we compare our observations with temperature-dependent trends seen in nanosecond photodesorption and with subpicosecond-pulse desorption of CO from Cu and Ru. The latter comparisons reveal a trend in the dynamics that appears to correlate with the electronic structure of the adsorbate−substrate complex.

As noted in the Introduction, the overall photodesorption process is modeled as two distinct steps: (i) vibrational excitation and (ii) desorption. We have chosen to describe the adsorbate excitation using the empirical friction model. This approach has been shown repeatedly to be an effective empirical model for subpicosecond photodesorption[19,22,23,33,38] and is a good starting point for discussing mechanisms.[1,5] In this model, coupling of the substrate excitation to the adsorbate is understood to be a frictional coupling; the electronic and lattice degrees of freedom couple independently to the adsorbate with strengths given by the frictional coupling coefficients, η_{el} and

η_{ph}, respectively. The rate of energy transfer to the adsorbate is governed by

$$\frac{dU_{ads}}{dt} = \eta_{el}(U_{el} - U_{ads}) + \eta_{ph}(U_{ph} - U_{ads}) \qquad (1)$$

where U_{ads} is the energy of the adsorbate (along the reaction coordinate), and U_{el} and U_{ph} are the energies that the adsorbate would possess if it were equilibrated to the electronic and lattice temperatures, T_{el} and T_{ph}, respectively. The adsorbate is treated within a one-dimensional harmonic-oscillator approximation, such that the average energy of an oscillator at temperature T_q is

$$U_q = \frac{h\nu_{rc}}{\exp(h\nu_{rc}/k_B T_q) - 1} \qquad (2)$$

with ν_{rc} the vibrational frequency characteristic of motion along the reaction coordinate. We consider here the molecule−surface stretch, with a calculated frequency $\nu_{rc} = 10^{13}$ s^{-1};[29] in previous work, the choice of frequency was found to have only a minor effect,[39] so, in principle, a different mode such as frustrated rotation[15] could be substituted without changing the overall conclusions.

The desorption step is modeled as a one-dimensional activation-energy barrier crossing governed by an Arrhenius expression, the Polanyi−Wigner rate equation for first-order desorption,

$$R_d = -d\theta/dt = \theta\nu_{PW} \exp[-E_a/k_B T_{ads}] \qquad (3)$$

where θ is the coverage, t is time, E_a is the desorption activation energy, and ν_{PW} is the prefactor. The prefactor is often treated as an adjustable parameter, although it may also be defined in terms of other system parameters for purely electron-mediated desorption.[19,33,39] Because we seek to include phonon-based processes, the electron-only form cannot be used in the model. One possibility is to assume separate activation energies and prefactors for electron-mediated and phonon-mediated desorption, modeling the problem as two separate populations desorbing by different means with different rates, but there is currently no evidence to support the additional parameters that would be required to implement such a model. We instead opt for the simpler, conventional approach where E_a and ν_{PW} are used as effective desorption parameters describing all possible mechanisms, including contributions from both electrons and phonons.[5,23,33] There are several cases where E_a from TPD data have been used successfully in simulating photodesorption with an empirical friction model.[33,34,39] Due to strong repulsions between adsorbate molecules,[26,41] E_a and ν_{PW} for CO/Pd(111) change dramatically with coverage according to TPD, even over the first 0.33 ML.[35] The change in E_a across this coverage range, which is not as rapid as the change in ν_{PW}, is further supported by molecular-beam experiments.[42] As a first, reasonable attempt to construct a phenomenological model, we neglect coverage and time dependence in the desorption parameters; variations in the desorption rate occur only through changes in T_{ads}. As will be shown below, both E_a and ν_{PW} must be maintained within ranges consistent with TPD to achieve reasonable agreement with experiment.

As described in detail elsewhere,[39] the response of the Pd to photoexcitation is simulated using the two-temperature model,[43] in which the substrate electrons and phonons are approximated as temperature baths T_{el} and T_{ph}, respectively. The evolution of these baths in terms of time, t, and depth
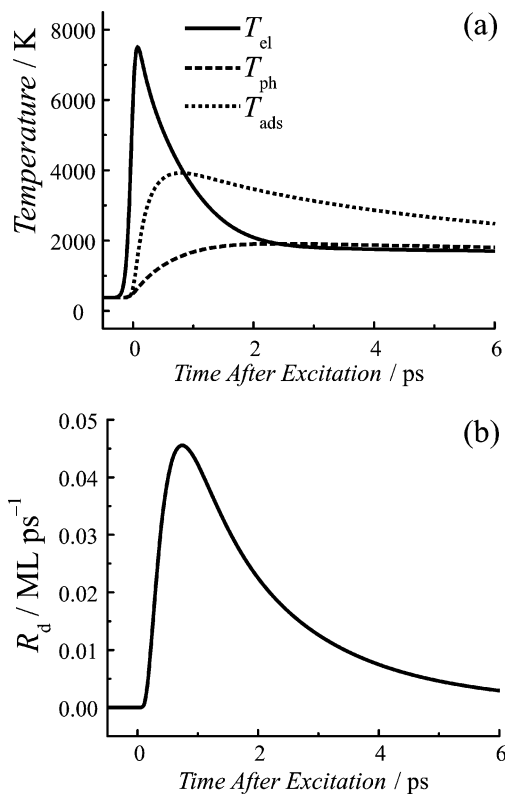

Figure 6. (a) Electronic (T_{el}), phonon (T_{ph}), and adsorbate (T_{ads}) temperatures following the absorption of a pair of pulses with zero delay. The temperatures are calculated at initial temperature $T_i = 375$ K using friction parameters found in Table 1 for $E_a = 1.43$ eV and $\nu_{PW} = 10^{13}$ s^{-1}. (b) Desorption rate resulting from the calculated T_{ads}.

into the crystal, z, is described by two coupled differential equations,

$$C_{el}\frac{\partial}{\partial t}T_{el}(t,z) = \frac{\partial}{\partial z}\kappa\frac{\partial}{\partial z}T_{el}(t,z) - g[T_{el}(t,z) - T_{ph}(t,z)] + S(t,z) \qquad (4)$$

$$C_{ph}\frac{\partial}{\partial t}T_{ph}(t,z) = g[T_{el}(t,z) - T_{ph}(t,z)] \qquad (5)$$

where C_{el} and C_{ph} are the heat capacities of the electron and phonon heat bath, κ is the thermal conductivity, $S(t,z)$ is the laser heating source term, and g is the electron−phonon coupling coefficient. The source term is calculated by assuming a pair of pulses with peak fluences[39] of 7.45 and 10.59 mJ cm^{-2} for 2PC and temperature-dependence simulations. The time evolution of the electronic and lattice phonon temperature baths is shown in Figure 6, along with an example of the adsorbate response and time-dependent desorption rate simulated using coupling and desorption parameters determined as described in detail below.

We have considered four variations of the frictional coupling model where the adsorbate is coupled (i) only to phonons, (ii) only to electrons, (iii) to both phonons and electrons where both coupling coefficients are independent of temperature, and (iv) to both phonons and electrons where the electronic coupling coefficient is temperature-dependent. In what follows, we discuss the adequacy of these models in turn, moving from the simplest to the more complex. We find that the increase in complexity of the model is required to adequately simulate the observed effects.

To begin, we consider a model where the adsorbate is coupled to the photoexcitation only through phonon interactions (i.e.,
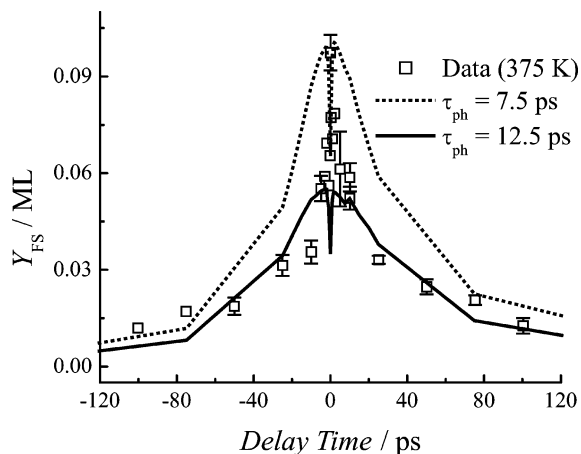
Figure 7. Experimental (symbols) and example simulated (lines) first-shot yields from 2PC experiments at $T_i = 375$ K. Coupling to electrons was neglected, with coupling to lattice phonons treated as a constant coupling time $\tau_{ph} = \eta_{ph}^{-1}$. Desorption parameters for the example simulations are $E_a = 1.43$ eV and $\nu_{PW} = 9.49 \times 10^{14}$ s^{-1}.

$\eta_{el} = 0$ in eq 1). Such a model might be expected to perform well on the basis of the results for CO/Ru(001),[33] where a phonon coupling model was found to explain the slow 2PC relaxation rate similar to the slow component we observe for CO/Pd(111). To test this model, η_{ph}, E_a, and ν_{PW}, were varied to best simulate the 2PC results. The desorption parameters in eq 3 were varied independently without regard to the peak desorption temperature in TPD;[39] however, a good fit could not be obtained. Results with $E_a = 1.43$ eV and $\nu_{PW} = 9.49 \times 10^{14}$ s^{-1} (Figure 7) exemplify the failings of this model. A coupling time of $\tau_{ph} = \eta_{ph}^{-1} = 7.5$ ps can reasonably reproduce the maximum yield in the 2PC; however, the maximum is slightly offset from zero delay due to a brief rise time that is not observed (but possibly difficult to resolve) in the experiment.[33,39] Furthermore, and more significantly, the width of the simulated correlation is much too broad. Optimizing the simulations for the slower time scale of the 2PC ($\tau_{ph} = 12.5$ ps in Figure 7) can simulate the slow decay of the wings in the 2PC signal but completely fails to reproduce the sharp peak near zero delay. The simulations shown are for $T_i = 375$ K, but similar results were obtained at 200 K. Different combinations of activation energies and prefactors also led to the same general trends. Therefore, a strictly phonon-mediated mechanism cannot describe the desorption process in this system.

In a second model, simulations were performed with a temperature-independent coupling to electrons, i.e., with η_{el} constant in eq 1. As in the phonon-only model, E_a and ν_{PW} are treated as unconstrained adjustable parameters. The resultant 2PC simulations are significantly narrower and a much better match for the experimental data than the phonon-only model. However, the temperature dependence of the 2PC is not well-reproduced by this model; we find that it can reasonably approximate the 2PC at one temperature, but the same parameters do not correctly predict the yields at different temperatures. A third model, which added coupling to phonons similarly failed to model the temperature dependence of the yield with a single set of coupling and desorption parameters. Lacking *a priori* knowledge of the coupling and desorption parameters, we do not think it reasonable to assume a different parameter set for each initial temperature.

Our fourth and final model is thus an extension of a model used in our previous work[34,39] and first proposed by Höfer and co-workers.[44-46] These models include a temperature dependence in the electronic friction that significantly improves the

empirical friction model description of ultrafast photodesorption and photoinduced diffusion, at least in some systems. Here, the temperature dependence of η_{el} is introduced through a power-law parametrization,

$$\eta_{el} = \eta_0 + \eta_\beta T_{el}{}^\beta \qquad (6)$$

where β, η_0, and η_β are phenomenological parameters. The physical significance of the temperature dependence is addressed below and in our previous work,[34,39] as well as that of Höfer and co-workers.[44-46]

Allowing for coupling to lattice phonons introduces an ambiguity into this model. The parameter η_0, representing the low-temperature limit of the electronic friction, acts to regulate the "memory" of the excitation within the system and is critical for simulating the 2PC of electron-mediated desorption at delay times beyond ±5 ps in the DIMET system O$_2$/Pd(111).[34,39] However, the phonon coupling (η_{ph}) serves essentially the same purpose.[39] Because the correlated signal in the CO/Pd(111) 2PC experiment (Figure 5) persists at delay times an order of magnitude longer than those seen for O$_2$/Pd(111),[34,38,39] it is important to evaluate the possible role of coupling to Pd phonons, which has been invoked to explain similarly slow relaxation rates in CO/Ru(001).[33] Thus, in the absence of other evidence, we have chosen to include η_{ph} and set $\eta_0 = 0$. This model therefore incorporates three adjustable coupling parameters, η_β, β, and η_{ph}, and two adjustable desorption parameters, E_a and ν_{PW}, for a total of five parameters (i.e., two more than were used in the single coupling mode models and one more than was used in the model that involved temperature-independent coupling to both electrons and phonons).

Figure 8 shows the results of simulations conducted using the temperature-dependent model with $E_a = 1.43$ eV and $\nu_{PW} = 10^{13}$ s^{-1}. A broad range of values for η_β, β, and η_{ph}, were employed at two different starting temperatures (200 and 375 K), and the simulated and experimental 2PC were compared to calculate a global goodness-of-fit parameter for each set of trial values:

$$\chi^2 = \chi^2_{200\,K} + \chi^2_{375\,K} \qquad (7)$$

where χ^2 at each initial temperature T_i is calculated according to

$$\chi^2_{T_i} = \sum_i (Y_{sim,i,T_i} - Y_{meas,i,T_i})^2 \qquad (8)$$

In eq 8, first-shot yields (Y) at each delay time, i, are compared from both simulations ("sim") and experimental measurements ("meas"). The friction parameters, listed in Table 1, that best fit the data at both temperatures with this choice of E_a and ν_{PW} slightly underestimate the peak yield at 200 K and slightly overshoot the experimental value at 375 K (Figure 8). In general, however, the shape and temperature dependence of the 2PC agrees well with experiment.

Significantly, the parameters chosen to best fit the 2PC data also quantitatively predict the observed trends in the other types of experiments. The first-shot yield, calculated at zero delay for a series of T_i, is in excellent agreement with the data; the values of the observed yields and their approximately linear increase with temperature are accurately simulated (Figure 3). Furthermore, the highly nonlinear fluence dependence (Figure 4) is reproduced (Table 1). The predicted power-law exponents ($n = 10.6$ and 8.2 for $T_i = 200$ and 375 K, respectively) exceed those measured (8.8 and 6.7; see Figure 4), but the disagreement
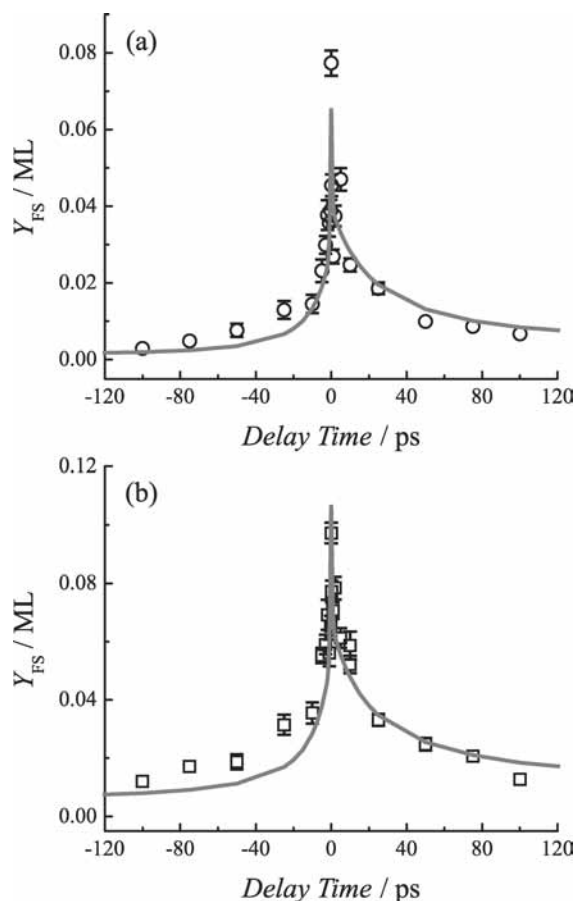
Figure 8. Experimental (symbols) and simulated (lines) first-shot yields from 2PC experiments with initial temperatures of (a) 200 K and (b) 375 K. Both temperature-dependent coupling to electrons and temperature-independent coupling to phonons were considered simultaneously.

TABLE 1: Optimized Parameters for Empirical-Friction Model ($\beta = 1.75$) and Predicted Photodesorption Properties

E_a (eV)	ν_{PW} (s^{-1})	η_β (s^{-1} K$^{-1.75}$)	η_{ph} (s^{-1})	T_i (K)	power-law n	peak T_{ads} (K)	R_d fwhm (ps)
1.29	1.0×10^{13}	4.24×10^5	3.3×10^{11}	200	8.7	3510	1.08
				375	6.7	3980	1.08
1.43	2.0×10^{13}	6.80×10^5	1.0×10^{12}	200	7.2	3890	0.60
				375	5.7	4370	0.61
1.43	1.5×10^{13}	3.80×10^5	2.0×10^{11}	200	10.1	3440	1.25
				375	7.8	3910	1.22
1.43	1.0×10^{13}	3.50×10^5	5.0×10^{10}	200	10.6	3450	1.79
				375	8.2	3930	1.66
1.43	7.5×10^{12}	4.00×10^5	1.0×10^{10}	200	9.9	3720	1.80
				375	7.7	4200	1.64
1.56	1.0×10^{13}	4.70×10^5	$\leq 10^{10}$	200	9.7	4000	1.48
				375	7.7	4490	1.35

is not severe given the uncertainty in the experimental values ($\sim$1.1 as stated earlier). It is also important to note that the simulations correctly reproduce the experimentally observed decrease in n with increasing T_i.

We have also varied E_a and ν_{PW} and find that their ranges are restricted by the constraints imposed by a global fit to the available data. To test the limits of their ranges, we performed simulations for numerous sets of E_a and ν_{PW} with β fixed at 1.75 and η_β and η_{ph} determined by minimizing χ^2 (eq 7). Values for E_a and ν_{PW} that gave reasonable agreement with the experimental results are listed in Table 1. It is important to note that these sets of values accurately simulate the observed trends, namely (i) the increase in the 2PC width (Figure 5) and (ii) the decrease in the fluence-dependence power-law exponent with increasing T_i (Figure 4). With $\nu_{PW} = 10^{13}$ s^{-1}, satisfactory global agreement with all experiments is achieved for E_a between 1.29 and 1.56 eV. Lower values for E_a result in 2PC widths that are substantially too broad and yields that change much too rapidly with T_i. Higher values for E_a result in a 2PC peak to baseline yield ratio significantly larger than observed, and beyond 1.7 eV the yields fall far short of experimental values. Raising (lowering) the prefactor ν_{PW} while maintaining a fixed E_a has effects similar to lowering (raising) E_a at fixed ν_{PW}. With $E_a =$ 1.43 eV, satisfactory global agreement with all experiments is achieved for ν_{PW} between 7.5×10^{12} and 2.0×10^{13} s^{-1}. Prefactors equal to or lower than 5×10^{12} s^{-1} fail to give sufficient yields and do not describe the temperature-dependent yields and 2PC. Prefactors higher than 2×10^{13} s^{-1} can be ruled out because above this value damping the excitation quickly enough to keep the yields at long delay times sufficiently low requires unrealistically short phonon coupling times ($\tau_{ph} = \eta_{ph}^{-1} \leq 1$ ps, much shorter than typical vibrational lifetimes on metal surfaces in the absence of coupling to EHPs[5,15]).

Although our values for E_a and ν_{PW} are determined from simulations of the photodesorption results, they are in quite reasonable agreement with those obtained from TPD. The activation energies in all successful simulations (Table 1) lie within the range observed in TPD over the first 0.33 ML.[35] The upper range, 1.56 eV, agrees with the zero-coverage limit of E_a. The value of 1.43 eV corresponds to the weighted average of $E_a(\theta)$ from $\theta = 0-0.33$ ML using the data from Guo et al.[35] and is close to their value at 0.20 ML. The prefactors in the photodesorption simulations, however, lie closer to those observed near saturation of the ($\sqrt{3} \times \sqrt{3}$)R30° overlayer (0.28–0.30 ML); they are roughly an order of magnitude lower than those derived from a leading-edge analysis of TPD spectra that gives $\nu_{PW} \sim 10^{14}$ s^{-1} at a coverage corresponding to $E_a =$ 1.4 eV.[35] This difference is likely not nearly as significant as its magnitude might suggest, considering that (i) ν_{PW} is notoriously difficult to determine to a high degree of accuracy from thermal desorption data alone and (ii) an order of magnitude difference in ν_{PW} corresponds to less than a 10% difference in E_a extracted from a TPD spectrum (e.g., using the Redhead equation[47,48]). In addition, there are physical considerations that imply that the prefactor in an Arrhenius model for ultrafast photodesorption desorption may be significantly lower than that in a strictly thermal desorption experiment. In connection with ultrafast photoinduced desorption of CO from Ru(001) Funk et al.[33] proposed that, because of the short time scales involved, the prefactor should be interpreted as an attempt frequency, which for their system was close to the molecule–surface vibrational frequency. In fact, we observe a similar agreement: $\nu_{PW} \approx \nu_{rc}$. In addition, the elevated temperatures during femtosecond photoinduced desorption compared to thermal desorption may result in a lowering of the effective prexponential due to a decrease in the entropic difference between the adsorbed and gas phases resulting from the enhanced mobility of the adsorbate.[49] In summary, our model for photodesorption with subpicosecond pulses requires an energetic barrier very similar to that seen in thermal desorption, and differences in the prefactor compared to that derived from a thermal desorption experiment may be due to differences in the time scale and temperature at which the desorption occurs.

The model makes quantitative predictions (Table 1) that give insight into the dynamics and could, in principle, be verified by future experiments. The predictions are substantially independent of E_a and ν_{PW} provided that these fall within the relatively narrow range that accurately simulates our measurements. First, the model predicts that the peak adsorbate

Temperature-Dependent Photoinduced Desorption

J. Phys. Chem. A, Vol. 111, No. 49, 2007 **12531**

temperatures are in the 3400−4000 K (3900−4500 K) range for $T_i = 200$ K (375 K). Second, the model predicts that the width of the desorption pulse, characterized as the fwhm of the R_d temporal profile, is between 0.6 and 1.8 ps (this should not be confused with the 2PC width). Surface-sensitive ultrafast spectroscopic probes of the adsorbate[32,50−53] could in principle monitor desorption time scales and temperature.

In all cases the simulations indicate that the desorption is driven by coupling to the electronic degrees of freedom of the substrate; qualitatively, this is expected given the strong subpicosecond decay in the 2PC measurement. The friction model simulations can be used to gain some degree of quantitative insight that goes beyond this basic qualitative understanding. Specifically, the simulations indicate that the coupling to the electronic degrees of freedom is quite strong. The optimal value for the electronic coupling coefficient η_β derived from the fitting is 3.5×10^5 s^{-1} K$^{-1.75}$. At the elevated electronic temperatures achieved in these experiments this corresponds to a fast coupling with $\tau_{el} = \eta_{el}^{-1}$ in the range of 500 fs. The strength of the coupling is reflected in the elevated temperature associated with the desorption coordinate T_{ads}, which reaches a maximum in the 4000 K range. Note that, though we can vary the model parameters and still achieve good fits, η_β varies over a fairly narrow range (Table 1), and is in all cases consistent with a strong interaction between the adsorbate and the substrate electrons.

The simulations also indicate that coupling to the lattice degrees of freedom does not play a role in driving the desorption. Rather, we find that the role of phonon coupling is limited to that of damping the excitation of the adsorbate. The reason for this can be deduced from Figure 6. Because strong electronic coupling is required to reproduce the observed yields and fast 2PC response, the simulation indicates a fast rise in the temperature of the desorption coordinate (T_{ads}, Figure 6) such that T_{ads} is higher than T_{ph} following the laser pulse excitation. Under these conditions, any coupling to the lattice can only act to cool the adsorbate. One to two picoseconds following excitation, when the substrate electrons cool and electronic coupling becomes less efficient (eq 6), the strength of the phonon coupling can determine the cooling rate of T_{ads} and, therefore, the "memory" of the vibrational excitation retained in the desorption coordinate. This memory, in turn, determines the slower decay time scale (∼40 ps) observed in 2PC; increasing the phonon coupling tends to decrease the memory of the adsorbate excitation and reduce the 2PC width. We find the best fit suggests a moderate coupling strength, with $\tau_{ph} = \eta_{ph}^{-1} = 20$ ps. However, there is a tremendous uncertainty in the phonon coupling strength. As shown in Table 1, relatively small changes in E_a and ν_{PW} result in η_{ph} values that span at least 2 orders of magnitude; the corresponding coupling times range from 1 to ≥100 ps[54] over the series of desorption parameters.

The moderating role of the lattice interaction can be seen in the relationship between η_{ph} and the desorption parameters shown in Table 1. For example, as E_a is increased, energy must be transferred more efficiently into the desorption coordinate to achieve sufficient yields. In the best-fit simulations, this increased efficiency with increasing E_a is achieved not by increasing the electronic coupling strength (which remains fairly constant); instead, the requisite increase in energy transfer is achieved by decreasing the phonon coupling strength η_{ph}. Over the E_a range that results in reasonable fits we find η_{ph} decreases from 3.3×10^{11} s^{-1} to a value that is less than or equal to 10^{10} s^{-1}, corresponding to an increase in τ_{ph} from 3 ps to ≥100 ps. A similar trend is seen with decreasing ν_{PW}. Thus, although it
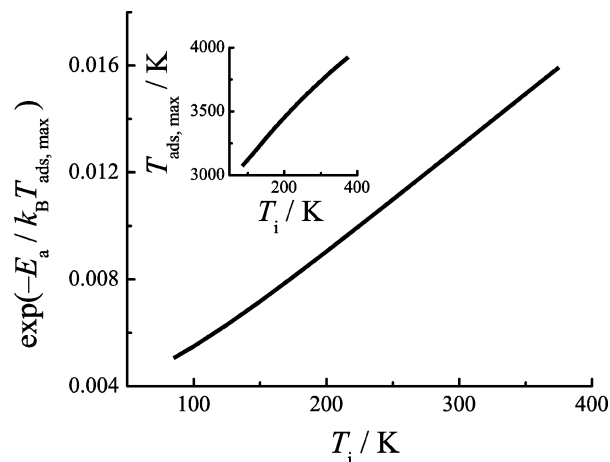

Figure 9. Estimate of the dependence of the peak desorption rate on initial temperature made by exponentiating the calculated maximum adsorbate (T_{ads}) temperature (eq 3) with $E_a = 1.43$ eV. Inset: maximum T_{ads} following excitation by a pair of pulses at zero delay calculated at different T_i with the friction parameters found in Table 1.

is clear that the model indicates that the CO molecules are heated through their interaction with the photoexcited electrons, and that interactions with the lattice do not contribute to driving the desorption but may play a moderating role, it is not possible to specify the strength of that moderating interaction with certainty.

It is perhaps surprising that an ultrafast process involving strongly excited electrons can be influenced so significantly by the initial substrate temperature (Figure 3). According to the two-temperature model simulations, the substrate is excited to a peak T_{el} that exceeds T_i by more than a factor of 10 (Figure 6). In comparison, varying T_i from 85 to 375 K seems insignificant. However, the observed T_i dependence can be understood in a straightforward manner based on the dependence of the adsorbate temperature on T_i and the activated nature of the desorption. Over the experimental range of T_i, the peak temperature of the adsorbate increases roughly linearly with T_i, as shown for zero delay in the inset in Figure 9. (We find the same approximately linear relationship at nonzero delays, even those far exceeding 100 ps.) A simple way to consider the consequences of this dependence upon T_i is to estimate the desorption rate at the peak temperature by substituting the calculated T_{ads} into the Arrhenius desorption rate (eq 3). In doing so we predict a nearly linear dependence of the desorption rate over the experimental T_i range (Figure 9) that strongly resembles the experimental and simulated temperature dependences (Figure 3). Thus, the essential physics behind the strong dependence of the desorption rate on the initial temperature is explained within the context of this simple model for an activated process driven by coupling to the electronic excitation of the substrate. The enhancement in photoyield with increasing initial temperature, and, as a result, the decrease in n and the broadening of the 2PC width, are the result of the thermal increase in the population of vibrationally excited states of the adsorbate−substrate system, which increases the probability of reaching the desorption continuum.

We are not aware of existing experimental studies of the temperature dependence of desorption in the subpicosecond photoexcitation regime where DIMET is possible. However, temperature-dependent yields have been observed in nanosecond-pulse photoinduced desorption of various adsorbates from semiconducting,[55] insulating,[56] and metal[57] surfaces. In these cases, enhancement of the yield with increasing initial temperature is similarly attributed to the increased probability of

excitation to the desorption continuum with an increase in the initial thermal population of excited adsorbate−substrate vibrational energy levels. A similar vibrationally assisted DIET mechanism was proposed for the photodesorption of benzene from Pt(111) by subpicosecond or subnanosecond pulses.[58] Taken together with these previous studies, our results indicate that thermal desorption in both the linear (single excitation, e.g., DIET) regime and nonlinear (multiple excitation, e.g., DIMET or "ladder climbing"[14]) regimes can be thermally assisted and are reasonably well-described by one-dimensional potential energy surfaces that are closely linked to those conventionally used to describe thermal desorption.

Carbon monoxide has been the target of subpicosecond photodesorption experiments on a number of other substrates with a variety of probe techniques,[23,24,32,33,36,50,59−63] but to our knowledge the only other surfaces for which desorption 2PC results have been reported are Ru(001)[33] and Cu(100).[23] The work on Cu(100) showed a highly nonlinear fluence dependence ($n = 8$) and a narrow 2PC (fwhm = 3 ps), and the desorption mechanism was assigned as electron-mediated friction. In contrast, the CO/Ru(001) experiments showed a broad correlation width (fwhm ∼20 ps) with a slightly smaller $n = 4.5$. In this case, the desorption is believed to be phonon-mediated. The hypothesized difference between Cu(100) and Ru(001) lies in the position of the CO $2\pi^*$ adsorbate resonance,[33] into which substrate electrons may be excited. A doublet resonance at 2.4 and 3.9 eV above the Fermi level (E_F) is observed for Cu(100),[64] and a resonance at 4.9 eV above E_F is detected on Ru(001).[65] On this basis Funk et al. estimated that in the Ru case there are not enough electrons of sufficient energy to excite the molecule−surface bond.[33] However, because electron-mediated energy transfer between the substrate and adsorbate can occur via direct coupling between the nuclear degrees of freedom and the EHPs,[15,19] the possibility that CO desorption from Ru(001) is due to electronic coupling driving ladder-climbing remains open.[14,33]

Both of the commonly proposed mechanisms for ultrafast pulse photodesorption, DIMET and ladder climbing, are consistent with the temperature-dependent friction model that best describes our results. On the one hand, it is possible that the photodesorption of CO from Pd(111) is driven by a resonantly enhanced process, i.e., that the DIMET mechanism plays a role. Qualitatively, we expect resonant enhancement to be more likely in the case of CO/Pd(111) than CO/Ru(001) because the $2\pi^*$ orbital should be more accessible to excited electrons given that (i) the CO $2\pi^*$ is nearly 1 eV closer to the Pd Fermi level,[66] (ii) the Pd d-band center is 1 eV higher than in Ru,[29] and (iii) the CO $2\pi^*$ width is expected to be significantly broader because CO favors a 3-fold hollow site on Pd(111) vs the on-top site on Ru(001).[29] The influence of the site dependence of the CO $2\pi^*$ width may be particularly significant: density-functional theory shows that on Pt, the width of the CO $2\pi^*$ resonance broadens with increasing coordination number and that a portion of the resonance actually extends *below* E_F for CO in the 3-fold hollow.[29] Thus we would expect coupling involving multiple electron transfers between the Pd and the CO $2\pi^*$ to be likely.

Alternatively, a ladder-climbing mechanism driven adiabatically on the molecular ground electronic state also is reasonable. Tully et al. have shown that electronic friction due to electron−hole pair transitions in the substrate can depend strongly on temperature.[15] In their calculations, this dependence on temperature is associated with the adsorbate vibrational motion and, therefore, is of a different physical origin than the electronic-

temperature dependence of diabatic coupling originally conceived in the development of the model we have employed.[19] However, the parametric description of the coupling strength we use (eq 6) may be seen as describing an adiabatic process. As a result, although we are confident that the excitation process is electron-mediated, the exact nature of the coupling remains an open question.

5. Conclusions

We have characterized the two-pulse correlation (2PC) and fluence dependence of the subpicosecond photodesorption of CO from a Pd(111) surface as a function of the initial substrate temperature (T_i). Lowering T_i increases the nonlinearity of the fluence dependence and reduces the 2PC width. This temperature dependence can be understood in terms of the initial degree of vibrational excitation in the adsorbate and adsorbate/surface modes. With increasing T_i, the desorption becomes more efficient because less energy needs to be added to drive the adsorbate over the desorption barrier. Furthermore, with increasing T_i, the population remains excited for longer times as the system cools, an effect that contributes to enhanced photodesorption efficiency. The temperature dependence is clearly illustrated through a simple experiment where T_i is varied from 85 to 375 K at zero pump−probe delay.

The concept of thermally assisted photodesorption is tested more formally by a phenomological model that fits all available experimental data with a single parameter set. The simulation results indicate that the desorption is driven by electronic coupling and that if lattice coupling is significant, it acts only to moderate the excitation of the adsorbate. The model indicates that a temperature-dependent electronic friction best describes our observations, consistent with resonantly enhanced coupling to the $2\pi^*$ molecular resonance. Systematic variation of the activation energy and prefactor for desorption within limited ranges indicates that the energy barrier to photodesorption is in good agreement with that found in thermal desorption experiments.

The limitations of our one-dimensional model come to bear when considering that EHP coupling with molecular vibrations is highly mode-dependent.[4,15,16] A more complete description of the process would involve a multidimensional model with the possibility of energy transfer between modes.[44] Additionally, the observed temperature-dependent friction may result from changes in the molecule−surface distance[15] or coupling among vibrational modes,[44] rather than a resonance enhancement. Despite these caveats, the model employed here has provided physical insight into the dynamics of the CO/Pd(111) interface and may serve as the foundation for further work on this system. Finally, direct measurements of the transient adsorbate temperature, the time scale for desorption, and activation energy would further elucidate the dynamics and provide a more stringent test of the adequacy of simple models.

References and Notes

(1) Frischkorn, C.; Wolf, M. *Chem. Rev.* **2006**, *106*, 4207.

(2) Avouris, Ph.; Walkup, R. E. *Annu. Rev. Phys. Chem.* **1989**, *40*, 173.

(3) Buntin, S. A.; Richter, L. J.; Cavanagh, R. R.; King, D. S. *Phys. Rev. Lett.* **1988**, *61*, 1321.

(4) Tully, J. C. *Annu. Rev. Phys. Chem.* **2000**, *51*, 153.

(5) Saalfrank, P. *Chem. Rev.* **2006**, *106*, 4116.

(6) Gadzuk, J. W. *Chem. Phys.* **2000**, *251*, 87.

(7) Menzel, D.; Gomer, R. *J. Chem. Phys.* **1964**, *41*, 3311.

(8) Redhead, P. A. *Can. J. Phys.* **1964**, *42*, 886.

(9) Antoniewicz, P. R. *Phys. Rev. B* **1980**, *21*, 3811.

(10) Marsh, E. P.; Gilton, T. L.; Meier, W.; Schneider, M. R.; Cowin, J. P. *Phys. Rev. Lett.* **1988**, *61*, 2725.

(11) Zhou, X. L.; Zhu, X. Y.; White, J. M. *Surf. Sci. Rep.* **1991**, *13*, 73.

(12) Busch, D. G.; Ho, W. *Phys. Rev. Lett.* **1996**, *77*, 1338.

(13) Misewich, J. A.; Heinz, T. F.; Newns, D. M. *Phys. Rev. Lett.* **1992**, *68*, 3737.

(14) Saalfrank, P.; Kosloff, R. *J. Chem. Phys.* **1996**, *105*, 2441.

(15) Tully, J. C.; Gomez, M.; Head-Gordon, M. *J. Vac. Sci. Technol. A* **1993**, *11*, 1914.

(16) Krishna, V.; Tully, J. C. *J. Chem. Phys.* **2006**, *125*, 054706.

(17) Morin, M.; Levinos, N. J.; Harris, A. L. *J. Chem. Phys.* **1992**, *96*, 3950.

(18) Cavanagh, R. R.; Heilweil, E. J.; Stephenson, J. C. *Surf. Sci.* **1994**, *299–300*, 643.

(19) Brandbyge, M.; Hedegård, P.; Heinz, T. F.; Misewich, J. A.; Newns, D. M. *Phys. Rev. B* **1995**, *52*, 6042.

(20) Kao, F.-J.; Busch, D. G.; Cohen, D.; Gomes da Costa, D.; Ho, W. *Phys. Rev. Lett.* **1993**, *71*, 2094.

(21) Gao, S.; Busch, D. G.; Ho, W. *Surf. Sci.* **1995**, *344*, L1252.

(22) Budde, F.; Heinz, T. F.; Kalamarides, A.; Loy, M. M. T.; Misewich, J. A. *Surf. Sci.* **1993**, *283*, 143.

(23) Struck, L. M.; Richter, L. J.; Buntin, S. A.; Cavanagh, R. R.; Stephenson, J. C. *Phys. Rev. Lett.* **1996**, *77*, 4576.

(24) Bonn, M.; Funk, S.; Hess, C.; Denzler, D. N.; Stampfl, C.; Scheffler, M.; Wolf, M.; Ertl, G. *Science* **1999**, *285*, 1042.

(25) Conrad, H.; Ertl, G.; Koch, J.; Latta, E. E. *Surf. Sci.* **1974**, *43*, 462.

(26) Bradshaw, A. M.; Hoffmann, F. M. *Surf. Sci.* **1978**, *72*, 515.

(27) Ohtani, H.; Van Hove, M. A.; Somorjai, G. A. *Surf. Sci.* **1987**, *187*, 372.

(28) Giessel, T.; Shaff, O.; Hirschmugl, C. J.; Fernandez, V.; Schindler, K.-M.; Theobald, A.; Bao, S.; Lindsay, R.; Berndt, W.; Bradshaw, A. M.; Baddeley, C.; Lee, A. F.; Lambert, R. M.; Woodruff, D. P. *Surf. Sci.* **1998**, *406*, 90.

(29) Gajdoš, M.; Eichler, A.; Hafner, J. *J. Phys. Condens. Matter* **2004**, *16*, 1141.

(30) Szanyi, J.; Kuhn, W. K.; Goodman, D. W. *J. Phys. Chem.* **1994**, *98*, 2978.

(31) Chuang, T. J. *Surf. Sci. Rep.* **1983**, *3*, 1.

(32) Prybyla, J. A.; Tom, H. W. K.; Aumiller, G. D. *Phys. Rev. Lett.* **1992**, *68*, 503.

(33) Funk, S.; Bonn, M.; Denzler, D. N.; Hess, C.; Wolf, M.; Ertl, G. *J. Chem. Phys.* **2000**, *112*, 9888.

(34) Szymanski, P.; Harris, A. L.; Camillone, N., III. *J. Chem. Phys.* **2007**, *126*, 214709.

(35) Guo, X.; Yates, J. T., Jr. *J. Chem. Phys.* **1989**, *90*, 6761.

(36) Kao, F.-J.; Busch, D. G.; Gomes da Costa, D.; Ho, W. *Phys. Rev. Lett.* **1993**, *70*, 4098.

(37) Prybyla, J. A.; Heinz, T. F.; Misewich, J. A.; Loy, M. M. T.; Glownia, J. H. *Phys. Rev. Lett.* **1990**, *64*, 1537.

(38) Misewich, J. A.; Kalamarides, A.; Heinz, T. F.; Loy, M. M. T. *J. Chem. Phys.* **1994**, *100*, 736.

(39) Szymanski, P.; Harris, A. L.; Camillone, N., III. *Surf. Sci.* **2007**, *601*, 3335.

(40) Kwiet, S.; Starr, D. E.; Grujic, A.; Wolf, M.; Hotzel, A. *Appl. Phys. B—Lasers Opt.* **2005**, *80*, 115.

(41) Glassey, W. V. *Surf. Sci.* **2006**, *600*, 173.

(42) Engel, T.; Ertl, G. *J. Chem. Phys.* **1978**, *69*, 1267.

(43) Anisimov, S. I.; Kapeliovich, B. L.; Perel'man, T. L. *Sov. Phys. JETP* **1974**, *39*, 375.

(44) Güdde, J.; Höfer, U. *J. Phys. Condes. Matter* **2006**, *18*, S1409.

(45) Stépán, K.; Dürr, M.; Güdde, J.; Höfer, U. *Surf. Sci.* **2005**, *593*, 54.

(46) Stépán, K.; Güdde, J.; Höfer, U. *Phys. Rev. Lett.* **2005**, *94*, 236103.

(47) de Jong, A. M.; Niemantsverdriet, J. W. *Surf. Sci.* **1990**, *233*, 355.

(48) Redhead, P. A. *Vacuum* **1962**, *12*, 203.

(49) Zhu, X. D.; Rasing, T.; Shen, Y. R. *Chem. Phys. Lett.* **1989**, *155*, 459.

(50) Bonn, M.; Hess, C.; Funk, S.; Miners, J. H.; Persson, B. N. J.; Wolf, M.; Ertl, G. *Phys. Rev. Lett.* **2000**, *84*, 4653.

(51) Bauer, M.; Lei, C.; Read, K.; Tobey, R.; Gland, J.; Murnane, M. M.; Kapteyn, H. C. *Phys. Rev. Lett.* **2001**, *87*, 025501.

(52) Fournier, F.; Zheng, W.; Carrez, S.; Dubost, H.; Bourguignon, B. *J. Chem. Phys.* **2004**, *121*, 4839.

(53) Lane, I. M.; King, D. A.; Liu, Z.-P.; Arnolds, H. *Phys. Rev. Lett.* **2006**, *97*, 186105.

(54) In this case, 100 ps represents a lower bound; coupling times shorter than 100 ps resulted in poorer fits, and much longer coupling times gave results essentially indistinguishable from those at 100 ps.

(55) Xin, Q.-S.; Zhu, X.-Y. *Chem. Phys. Lett.* **1997**, *265*, 259.

(56) Thiel, S.; Klüner, T.; Wilde, M.; Al-Shammery, K.; Freund, H.-J. *Chem. Phys.* **1998**, *228*, 185.

(57) Rao, R. M.; Beuhler, R. J.; White, M. G. *J. Chem. Phys.* **1998**, *109*, 8016.

(58) Arnolds, H.; Levis, R. J.; King, D. A. *Chem. Phys. Lett.* **2003**, *380*, 444.

(59) Cai, L.; Xiao, X.; Loy, M. M. T. *Surf. Sci.* **2000**, *464*, L727.

(60) Deliwala, S.; Finlay, R. J.; Goldman, J. R.; Her, T. H.; Mieher, W. D.; Mazur, E. *Chem. Phys. Lett.* **1995**, *242*, 617.

(61) Fournier, F.; Zheng, W.; Carrez, S.; Dubost, H.; Bourguignon, B. *Phys. Rev. Lett.* **2004**, *93*, 249602.

(62) Fournier, F.; Zheng, W.; Carrez, S.; Dubost, H.; Bourguignon, B. *Phys. Rev. Lett.* **2004**, *92*, 216102.

(63) Roeterdink, W. G.; Backus, E. H. G.; Kleyn, A. W.; Bonn, M. *Phys. Rev. Lett.* **2004**, *93*, 249601.

(64) Rogozik, J.; Dose, V.; Prince, K. C.; Bradshaw, A. M.; Bagus, P. S.; Hermann, K.; Avouris, Ph. *Phys. Rev. B* **1985**, *32*, 4926.

(65) Benndorf, C.; Bertel, E.; Dose, V.; Jacob, W.; Memmel, N.; Rogozik, J. *Surf. Sci.* **1987**, *191*, 455.

(66) Johnson, P. D.; Wesner, D. A.; Davenport, J. W.; Smith, N. V. *Phys. Rev. B* **1984**, *30*, 4860.